Accepted Manuscript

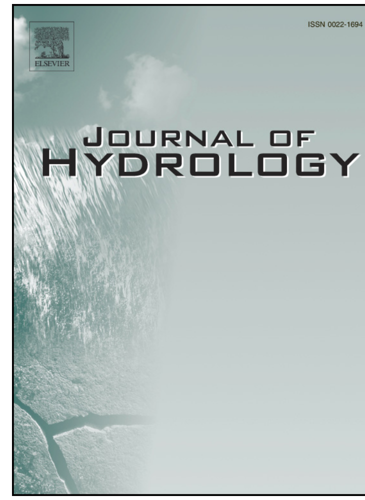

Investigation on the Use of Geomorphic Approaches for the Delineation of Flood Prone Areas

Salvatore Manfreda, Fernando Nardi, Caterina Samela, Salvatore Grimaldi, Angela Celeste Taramasso, Giorgio Roth, Aurelia Sole

PII: S0022-1694(14)00469-7
DOI: http://dx.doi.org/10.1016/j.jhydrol.2014.06.009
Reference: HYDROL 19683

To appear in: *Journal of Hydrology*

Received Date: 26 February 2014
Revised Date: 15 May 2014
Accepted Date: 7 June 2014

Please cite this article as: Manfreda, S., Nardi, F., Samela, C., Grimaldi, S., Taramasso, A.C., Roth, G., Sole, A., Investigation on the Use of Geomorphic Approaches for the Delineation of Flood Prone Areas, *Journal of Hydrology* (2014), doi: http://dx.doi.org/10.1016/j.jhydrol.2014.06.009

Investigation on the Use of Geomorphic Approaches for the Delineation of Flood Prone Areas

Salvatore Manfreda (1), Fernando Nardi (2), Caterina Samela (1), Salvatore Grimaldi (3), Angela Celeste Taramasso (4), Giorgio Roth (4) and Aurelia Sole (1)

(1) University of Basilicata, Potenza, Italy.

(2) University for Foreigners of Perugia, Perugia, Italy.

(3) Tuscia University, Viterbo, Italy.

(4) University of Genova, Genova, Italy.

Corresponding author:

Salvatore Manfreda,

E-mail: salvatore.manfreda@unibas.it,

Tel: +39 0971 205140; Fax: +39 0971 205160

Reviewed and resubmitted to Journal of Hydrology

(14/05/14)

Abstract

Three different geomorphic approaches to the identification of flood prone areas are investigated by means of a comparative analysis of the input parameters, the performances and the range of applicability. The selected algorithms are: the method proposed by Manfreda et al. (2011) based on a modified version of the Topographic Index (TI_m); the linear binary classifier proposed by Degiorgis et al. (2012), which uses different geomorphic features related to the location of the site under exam with respect to the nearest hazard source; the hydro-geomorphic method by Nardi et al. (2006) simulating inundation flow depths along the river valley with the associated extent of surrounding inundated areas. Comparison has been carried out on two sub-catchments of the Tiber River in Central Italy. The simulated flooded areas, obtained using the selected three methods, are evaluated using as a reference the Tiber River Basin Authority standard flood maps. The aim of the research is to deepen our understating on the potential of geomorphic algorithms and to define new strategies for prompt hydraulic risk mapping and preliminary flood hazard graduation. This is of foremost importance when detailed hydrologic and hydraulic studies are not available, e.g., over large regions and for ungauged basins.

Keywords: flood hazard, DEM, terrain analysis, Tiber River, ungauged basins.

1 Introduction

The identification of flood prone areas is a critical issue that is becoming more challenging and pressing for our society (e.g., Sivapalan et al., 2012; Di Baldassarre et al., 2013a; Di Baldassarre et al., 2013b). Both public administrators and private companies (e.g., insurance companies) call for the development of new tools and strategies for prompt risk identification and mapping over large regions.

In the last few decades, the scientific community developed significant efforts to improve techniques for the detection of areas exposed to the flood hazard and, nowadays, there are several hydrologic and hydraulic modelling approaches that are regularly used for practical applications (e.g., Norman et al., 2001; Grimaldi et al., 2013). Those standard models are classified according to their geometric and physical representation of the flood domain (e.g., grid cell or triangular irregular networks) and physical dynamics (e.g., 1D and 2D models). Physically based 2D models are able to describe the inundation hydrodynamics, allowing the mapping of flow depth and extent at the scale of the single building and down to the scale of micro-topographic and vegetation features (e.g., Cobby et al., 2003; Kim et al., 2011). Nevertheless, 2D flood models are computationally intense and require a significant amount of data and parameters values to describe the riverbed and floodway morphology as well as the surface roughness. This poses a challenging problem for their calibration and validation (Horritt and Bates, 2002; Di Baldassarre et al., 2009).

Notwithstanding the limitation of these models, there are several attempts to provide a global flood mapping collecting all available information (e.g. Dilley et al., 2005; Moel et al., 2009) or using large scale physically based models of rainfall-runoff and river routing (e.g. Pappenberger et al., 2012; Winsemius et al., 2013). Even if the full mosaic is not available yet, because of the limitations in the resolution of the products and the scale of the river basins considered, it may be extremely useful in reinsurance, large scale flood preparedness and emergency response (e.g. Kappes et al., 2012).

In order to overcome modelling limitations, a significant effort is oriented in the optimization of the existing algorithms for global flood mapping. In this contest, it is interesting to recall the recent work by Lamb et al. (2009) that suggested the use of technology from the computer graphics industry to accelerate a 2D diffusion wave flood model that have been used in several countries in Europe. Nevertheless, a comprehensive and detailed flood map at the global scale is still lacking.

On the other end, the river basin morphology intrinsically contains an extraordinary amount of information on flood-driven erosion and depositional phenomena, constituting a useful indicator of the flood exposure of a given area (e.g., Arnaud-Fassetta et al., 2009). These information may be used to enhance our ability to identify the portion of a river basin frequently submerged or extend information extractable from hydraulic simulation. In fact, the terrain morphology plays a central role in flood waves behaviour in a fundamental interplay that govern the landscape evolution across multiple spatial and temporal scales (e.g., Tucker et al., 2001; Tucker and Whipple, 2002). Following this theoretical principle, several authors have shown that the delineation of flood prone areas at the large scale can be carried out using simplified methods that rely on basin geomorphologic feature characterization (e.g., McGlynn and Seibert, 2003; Gallant and Dowling, 2003; Dodov and Foufoula-Georgiou, 2006). This kind of applications were originally hampered by the scarcity of detailed topographic data, but the advent of new technologies to measure topographic surface elevation (e.g., GPS, SAR, SAR interferometry, and laser altimetry), combined with the growing power of computers and the development of Geographic Information Systems (GIS), has given a strong impulse to the development of geomorphic approaches for valley bottoms identification using Digital Elevation Models (DEMs) as main data source.

We should be aware that while the first class of approaches (hydrologic and hydraulic) are able to appropriately identify and delimitate flood hazard areas, the second class (geomorphologic) are useful in ungauged condition to preliminary identify flooded areas.

In this work, we selected three different approaches for DEM-based flood prone areas identification that are hereafter briefly introduced: the modified Topmodel index approach by Manfreda et al.

(2011), a linear binary classifier by Degiorgis et al. (2012, 2013) and a inundation hydro-geomorphic characterization algorithm by Nardi et al. (2006, 2013). For simplicity, they will be named Geomorphic Method 1 (GM1), GM2 and GM3, respectively.

GM1 is based on the topographic index by Kirkby (1975), defined as ln(A_d/tanβ), as a function of the local upslope contributing area (A_d) and the local slope (tanβ). This index, as representative of the runoff production and storage mechanism, is a good indicator of frequently saturated areas as well as flood-prone areas, as recently investigated by Manfreda et al. (2011) that propose an improved index by changing the relative weight of the drained area with respect to the local slope introducing an exponent n (n<1) for the term A_d. This exponent was introduced in order to provide a measure of the relative value assumed by the hydraulic radius (~A_d^n) in a given point that represents a better descriptor of flood exposure. This index was used to develop a simplified procedure for the identification of flood-exposed areas.

Expanding the idea of using morphological indices for the description of flood prone areas, Degiorgis et al. (2012) investigated the relationship between several morphological features and flood hazard at the catchment scale using linear binary classifiers. Such procedure, here named GM2, is based on five selected morphologic features derived from DEMs. According to this work application, the best-performing feature is the difference in elevation between the location under exam and the downstream river node to which the site is hydrologically connected.

The GM3 estimates the variable water level along the river network and, by evaluating the elevation difference with surrounding areas, identifies the flooded area. This hydro-geomorphic algorithm, representing an extension of the geomorphic constant water level method by Williams et al. (2000), is based on the principle that flood-related erosional and depositional processes shaped the floodplain itself. As a result, the energy associated to these physical river flow phenomena is expressed in elevation terms to identify flood prone areas along fluvial valleys.

The three above-mentioned studies laid the groundwork for the present research that tackles the problem of the identification of the dominant topographic controls on the extend of flood prone-areas, where inundation is most likely to happen. This research question motivates this work that, by investigating the outcomes of the three selected techniques on two sub-catchments of the Tiber River in Central Italy, provides a useful discussion for understanding the simulated flooded areas behaviour as a function of the morphological indices. The aim is to better comprehend the potential and limitations of each algorithm to identify the most suitable geomorphic parameters and modelling approaches for the delineation of flood prone areas over large regions.

2 The study area and dataset: the Tiber River in Central Italy

The Tiber River originates from the Apennine Mountains in Emilia-Romagna (Fumaiolo mountain, 1407 m a.s.l.) and flows for 405 km in a generally southerly direction through Umbria and Lazio towards the Tyrrhenian Sea. It is the largest river basin in central Italy with a drainage area of 17.375 km^2 (Figure 1).

The Tiber River Basin Authority (TRBA) plan reports that the dominant land use for the basin is agriculture that covers about 53% of the surface, while approximately 39% is forested and 5% is urbanized. Its mean discharge at the outlet is approximately 230 m^3/sec, while the highest historical flood discharge was recorded in 1598 with a peak flow of about 4000 m^3/sec at the outlet (e.g., Calenda et al., 2005). This extraordinary value, corresponding to an estimated return period of 500year, have been reconstructed starting from the ten surviving flood markers that commemorate the 1598 flood.

For the purpose of this work, the study area is represented by the upper Tiber River basin, which is characterized by a complex topography that is mainly hilly with elevation ranging from 100 to 1500 m a.s.l.. The selected sub-catchments are: the upper Tiber River, with an area of about 5000 km^2, and the Chiascio River (one of the main left tributaries of Tiber River), with a drainage area of approximately 727 Km^2. See Figure 1 for the geographic and topographic setting of the two selected study basins.

Finally, it is extremely instructive to provide a preliminary description of the alluvial plain based on the geological information available over the area. This area may be considered as the maximum extend for any study related to flooding process. In fact the three formations that may be considered part of the river system from the geological point of view identify a significant portion of the river basin (see Figure 2) that do not necessarily correspond with the exposed to flood inundation under the scenario considered in the present work.

2.1 Standard flood maps

Several hydrologic and hydraulic studies, with different levels of detail, are available for this river basin. In particular, the "Piano di Assetto Idrogeologico" or PAI (Law Decree 183/1998 and 49/2010 implementing of the European Flood Directive 2007/60/EC) developed by TRBA contains flood hazard and risk maps based on detailed standard hydrologic and hydraulic models as well as guidelines and procedures for mitigation measures to be adopted for an integrated sustainable and safe urban development at the basin scale (TRBA PAI, 2010).

The TRBA PAI was developed using high precision bathymetric surveys of the channel surveyed as cross sections with average spacing interval of 200-400 meters, for a total of 1800 cross sections over a length of about 700 km. This detailed fluvial morphology was used as main input of a 1D hydraulic model simulating the effect of the design hydrographs considering return periods of 50, 200, and 500 years. Hydraulic simulation was carried out by the use of two models: the HEC-RAS (Hydrologic Engineering Center - River Analysis System – HEC-RAS, 2008) and the FRESCURE (FREe Surface CURrent Evaluation – TRBA 2010). The second one has been used in parallel with HEC-RAS for validation and comparison of the results.

A graphical layout of TRBA flood map is given in Figure 3, where: the dark blue line is the reference drainage network; red identify flood-prone areas derived from hydraulic studies of the standard PAI; the green areas are the so-called "marginal hazard areas", introduced by Degiorgis et al. (2013). It is necessary to underline that the marginal hazard areas are identified as the ensemble of the DEM cells that are: *i)* directly drained by the reference river network (dark blue of Figure 3.B); *ii)* not flowing through the streams depicted in light blue in Figure 3.B; *iii)* not recognized as prone to floods. This area is identified in order to define a study domain for the geomorphic methods proposed herein.

2.2 DEM and the stream network

The DEM used in this work is obtained from the HydroSHEDS dataset (hydrosheds.cr.usgs.gov/index.php), a remotely sensed elevation data product originated from the NASA Shuttle Radar Topography Mission (SRTM) at 3 arc-second resolution that is approximately 82 m. The Hydrosheds DEM is characterized by two sub-products: the VOID-filled (DEM–VOID) and the hydrologically CONditioned (DEM–CON) elevation model. In DEM–VOID the no-data voids are filled and the main elevation inconsistencies removed. DEM–CON is further conditioned to produce a river network coherent with the actual network (stream burning by decreasing the elevation of DEM cells along digitized river channels). Note that, since the conditioning process of the DEM-CON significantly alters the original elevation data, its use is limited only to the drainage network identification procedures, while the quantitative measures of morphologic characteristics (e.g., local slope, curvature or elevation difference between points) are derived from the original DEM–VOID data.

The reference drainage network, used by the three selected methods, is derived from the hydrologically conditioned DEM (DEM-CON) adopting the stream network delineation procedure proposed by Giannoni et al. (2005). Such algorithm stems from the classical slope-area method (Montgomery and Dietrich, 1988) and takes into account both the contributing area, A, and the local slope, S for the identification of channel initiation. In particular, channel heads are located at cells where the quantity AS^k exceeds a given threshold that, in the present case, was set equal to 10^5 m^2, while the channel path to the outlet is identified by following the steepest direction (Jenson and Domingue, 1988; Nardi et al., 2008).

3 Methods and their application

In the present section, the three selected methods (GM1, GM2, GM3), already introduced in Section 1, are described in more technical details in order to provide an overview of the input data and main characteristics and specification of the procedures (see Figure 4). As a general remark, the three methods have an increasing level of complexity and require different input. GM1 and GM2 are only based on geomorphic features derived from the DEMs, while the GM3 is a hydro-geomorphic approach and requires also information on the design flood peak at the basin outlet or the assignment of inundation depths for each channel node. This implies that the GM3 can be used starting from a preliminary hydrological study on the flood flow statistics for a given river basin and may be used without calibration, while GM1 and GM2 requires a calibration based on pre-existent flood maps for at least a subplot of the study area.

3.1 The Modified Topographic Index

The simulation of the catchment response to a precipitation event by means of topographic analysis dates back to Kirkby (1975) that proposed the topographic index, defined as $\ln(A_d/\tan\beta)$, as a function of the local upslope contributing area per unit contour (A_d) and the local slope ($\tan\beta$), in order to morphologically index the runoff production. The term "A_d" reflects the tendency of water to accumulate in certain locations of the basin, while the term "$\tan\beta$" represents the tendency of the gravitational force to route the water downhill. Therefore, the cells corresponding to high values of topographic index will tend to saturate first and are indicator of areas characterized by high specific contributing area, or limited slope. This index is commonly used to quantify topographic control on numerous hydrological processes and applications for water flow path estimation and soil moisture redistribution (Beven and Kirkby, 1979; Burt and Butcher, 1985; Moore et al., 1991).

This index is also a good flood-prone areas as recently highlighted by Manfreda et al. (2011) and Jalayer et al. (2014). In particular, Manfreda et al. (2011) proposed an improved index by changing the relative weight of the drained area with respect to the local slope introducing an exponent *n* (*n*<1) for the term A_d. The aim of such assumption is to provide a measure of the relative value assumed by the hydraulic radius in a given point. This principle, that generally refers only to the channelized flow, is roughly applied to the whole basin. By tuning the parameter *n*, the relative weight of the two terms of the expression may be modified, giving more or less relevance to local slope or to drainage area.

This index, named by the authors Modified Topographic Index, is defined as:

$$TI_m = \ln\left(\frac{A_d^n}{\tan(\beta)}\right) \quad [1]$$

Manfreda et al. (2011) observed that the portion of a basin exposed to flood inundation is generally characterized by a $\mathrm{TI_m}$ higher than a given threshold, τ. According to this concept, it is possible to develop a simple procedure to detect areas exposed to flood inundation by identifying the correct exponent and selecting the right threshold that optimizes the simulated flood map. This method was also used by Di Leo et al. (2011) to produce an automated procedure for the detection of flood prone areas, named r.hazard.flood (included in the GRASS GIS open source platform).

The calibration of the parameters τ and n can be obtained through the comparison between the flood prone area obtained with GM1 and the pre-existent flood inundation map obtained with hydraulic simulation using classical statistical measures of the performance of a binary classification test (e.g., Fawcelt, 2006).

This kind of approach is widely used in medicine tests, such as genetic tests and blood tests for various diseases or conditions, are far from infallible. A test can produce two kinds of errors: a false positive result (meaning that the test indicates presence of the disease when it is not there) or a false negative result (meaning that the test indicates absence of the disease when it is in fact present). In general, a population of tested individuals may be divided into four groups:

• True Positives (TP): those who test positive for a condition and are positive (i.e., have the condition),

• False Positives (FP): those who test positive, but are negative (i.e., do not have the condition),

• True Negatives (TN): those who test negative and are negative,

• False Negatives (FN): those who test negative, but are positive.

Given the above definition, the standard metrics used to identify the errors (Type I and Type II) and correct prediction:

- True positive rate: $r_{tp} = TP/(TP+FN)$;
- False positive rate (Error Type I): $r_{fp} = FP/(FP+TN)$;
- True negative rate: $r_{tn} = TN/(FP+TN)$;
- False negative rate (Error Type II): $r_{fn} = 1-TPR$.

In this case, we substitute the disease with the presence of a flood prone area and the condition with a specific morphological feature. A similar approach is also used in GM2.

In particular, the errors of Type I and II can be defined as:

$$r_{fp} = \frac{NS_{TRBA} \cap S_{GM1}}{NS_{TRBA}} \text{ (Type I)}, \; r_{fn} = \frac{S_{TRBA} \cap NS_{GM1}}{S_{TRBA}} \text{ (Type II)} \qquad [2]$$

where: S_{TRBA} and S_{GM1} describe the domain predicted as flooded by the TRBA and by the GM1; NS_{TRBA} and NS_{GM1} are the areas predicted as non-flooded by the hydraulic model and the GM1, respectively.

The sum of the two errors $(r_{fp} + r_{fn})$ represents an objective function that can be used for calibration purposes.

3.2 The linear binary classifiers

GM2 identifies areas subject to the flooding hazard through pattern classification techniques using several morphologic features. In particular, the linear binary classifier have been applied using one or a combination of two morphologic features.

In this work, the following DEM-derived quantitative morphologic features are taken into account:

1. the contributing area, A [m^2];

2. the surface curvature, $\nabla^2 H$ [-], defined as the Laplacian of the elevation;

3. the local slope, S [-], estimated as the maximum slope among the eight possible flow directions that connect the cell under exam to the adjacent cells;

4. the distance of each cell from the nearest stream, D [m], defined as the length of the path hydraulically connecting the location under exam to the nearest element of the drainage network;

5. the relative elevation to the nearest stream, H [m], defined as the difference in elevation between the cell under exam and the nearest element of the drainage network.

All the above features are displayed in Figure 5 for the portion of the Tiber River basin considered in the present study.

These features, related to the location of the site under exam with respect to the nearest hazard source (i.e., the nearest stream), are considered separately or mixed leaving the matching and weighting to an optimization procedure. A binary classifier was used to identify the best performing feature among the five above mentioned (e.g., Fawcelt, 2006).

Under such assumption, classification is obtained by using a moving threshold that discriminate between two portions of an area according to the specific value assumed by a given feature in a given point. This leads to the construction of the Receiver Operating Characteristics (ROC) curves that describes the value of the true positive rate as a function of the false positive rates by changing the threshold value. For any given threshold, the true positive rates, r_{tp}, defines the percentage of flooded area correctly identified, while the false positive rate, r_{fp}, defines how many incorrect flooded pixels have been identified by the specific threshold among all samples predicted to be non-flooded by TRBA. We recall that the r_{fp} was already introduced in the GM1 and was identified as overestimation error.

The Area Under the ROC Curve (also known as AUC) is used to compare the performances obtained with each morphologic feature. In general, an AUC equal to one represents the optimal condition for which r_{tp}= 1 and r_{fp} = 0. This measure is used only to evaluate the relative performances of each morphological feature, but not for the calibration of the threshold necessary to depict a map of flood-prone areas that will be obtained using a procedure similar to the one introduced in GM1.

From an operational point of view, the relationships between the selected morphologic features and the flood map are first calibrated at the sample scale and then applied to extend the hazard information at the basin scale.

3.3 Hydro-geomorphic method

GM3 is an automated GIS-based procedure, implementing a set of terrain analysis algorithms for flooded area delineation by linking a simplified inundation model with the geomorphic properties of the stream network and the fluvial buffer morphometry (Nardi et al., 2006; Nardi et al., 2013). The inundation model is defined as a function of the hydrologic characteristics of a predefined design flood event designed based on the flow peak discharge at the basin outlet.

This approach is based on three main steps:

1. DEM-based identification of the alluvial plain cross-sectional morphometry;
2. Identification of the inundation flow depth at the basin outlet corresponding to a predefined design flood peak discharge of given return period and estimation of the variable flow depths along the river network by using a power law scaling with the contributing area;
3. The absolute flood level elevation, assigned to each cross section, is compared to surrounding areas to identify the inundation extent that is the hydro-geomorphic flooded area.

The main input parameters of the method are the DEM and the design outlet flood discharge (Q_o) that may be obtained from stream flow records, post flood field measurements or statistical flood frequency analyses.

In Step 1 a sample set of cross sections are automatically extracted from the DEM to adequately represent the morphology. In this phase, the simulated river network is further simplified removing meanders that may alter the cross sections description.

Step 2 is based on the estimation of a variable flow level or flood stage (h) that is quantified for each stream cell as function of the contributing area (A), by using the hydraulic scaling relation proposed by Leopold and Maddock [1953]:

$$h = aA^b \tag{3}$$

where h is the water depth [m], A is the contributing area at the cell [m^2], and a [m^{1-2b}] and b [-] are the power law coefficient and exponent, respectively.

The flood stages h are typically not available at a sufficient number of locations for a proper calibration of a and b parameters. For this reason, GM3 implements a DEM-based algorithm for the estimation of the variable flood stage along the stream network that makes use of a predefined peak discharge value for the outlet. The corresponding peak values along the entire stream network are obtained by scaling the peak discharge through the explicit equation of the Geomorphic Instantaneous Unit Hydrograph (GIUH) method. Once the peak discharge is defined for a selected location, the corresponding water level is estimated using the uniform flow discharge equation in the Manning form.

The water level is, then, derived at a number of locations in the stream network to provide paired values of h and A. Those values are plotted on a log-log plot to estimate the best fitting line. Resulting a and b parameters, thus, represent respectively the intercept and slope of the simulated hydraulic scaling relation (Equation 3). The estimated water level is compared to the elevation of neighbouring cells defining the potentially inundated area.

In this way the climatic and hydrologic regime of the region is enforced into the model (the GIUH equation uses as input parameters the design rainfall intensity and the peak discharge at the outlet) following the theoretical principle of the original work: the floodplain extracted from DEMs by capturing the topographic signature of historical flood processes (Nardi at al., 2006; Nardi et al., 2013). In fact, GM3 performs the floodplain delineation in hydrogeomorphic terms by filtering flood prone areas as respect to the specific flood flow height associated to the pour point of the corresponding basin and not in geometric terms.

4 Application and results

The outcomes of the three methods are presented and investigated using as reference dataset the standard flood inundation maps of the TRBA, computed for a return period of 200 years. Maps provided by the TRBA may be affected by errors due to the modelling assumptions, survey errors, infrastructures, etc., but still represent the results of the most intensive and detailed study that is the actual best available information on flood hazard for the specific area.

Each algorithm has been calibrated using the same procedure originally suggested by the authors of the methods. Nevertheless, the domain of study is limited to the marginal hazard areas in all procedures and also the final comparison is made using common error metrics in order to provide a common ground of comparison. It is necessary to remark that methods have significant differences in their philosophy and calibration procedures that may somewhat influence the results. In fact, the GM1 and GM2 were numerically calibrated using objective functions, while parameters downstream hydraulic geometry relationship in GM3 are tuned by selecting the final calibration set, among the different combinations satisfying the enforcement of the predefined outlet flood flow level of given return period, by means of a qualitative comparison with the standard TRBA flood map.

In the following, we provide a description of the application of each procedure that was made independently from each other.

4.1 The modified topographic index

The calibration of the two parameters n and τ of the GM1 was performed using only the portion of the basin within the marginal hazard areas, which provides a description of the flooded area along the main river and a portion of few tributaries. To this end, an iterative procedure was used, varying both the values of n and τ, searching for the minimum of the sum of the two error functions ($r_{fp}+$ r_{fn}) previously introduced (see Section 3.1). Comparison is made between the areas with topographic index (described in Figure 6.A) higher that the given threshold with the hazard maps provided by the TRBA searching for the parameters values that minimize the total error (($r_{fp}+r_{fn}$).

The resulting parameters are:

- exponent n=0.020; threshold τ=3.1 for the Upper Tiber River basin, where the error $r_{fn}=$ 0.062 and $r_{fp}=0.387$;
- exponent n=0.00; threshold τ=2.6 for the Chiascio River basin, where the error $r_{fn}=0.098$ and $r_{fp}=0.486$.

Once the optimal parameters are calibrated over the marginal hazard areas, they are used to map areas exposed to flood inundations over the portion of the sub-catchments not included in the original River Basin Authority PAI, as shown in Figure 6.B. In this case, calibrated parameter values evidenced that the rule of the slope is a dominant one with respect to that of the contributing area, because the parameter n obtained from the calibration is almost zero in both cases.

It is necessary to remark that our previous experiences highlighted that the application to rivers featuring low slope provides higher errors. This is confirmed in the present application where the selected area cover an area with a gentle slope, but the choice was influenced by the need to select an area for models inter-comparison. In particular, GM3 imposed the constrain on the selection of the study area that could not be extended on basins with an area lower than 500km^2.

4.2 The linear binary classifier

The morphometric features, introduced in Section 3.2, have been used as a single feature or in combination of two. The first step of GM2 is characterized by the distinction between flood-prone areas (class 1) and marginal hazard areas (class 0). To this end, data are first normalized, so that corresponding values lie between -1 and 1.

GM2 was first adopted in a single feature framework and later in a two-features basis. ROC curves, defined as the set of pairs (r_{fp}, r_{tp}) obtained by varying the threshold of the classifier, were derived for each feature in order to select the most efficient feature (seeFigure 7). The optimal normalized threshold value is obtained by minimizing the sum of the false positive rate and the false negative rate r_{fp} + (1 - r_{tp}) assigning equal weights to the two rates. It is necessary to remark that each data point is assigned to the class 0 if the feature is above the threshold, and to the class 1 if it is under the threshold for the classifiers based on H, D, and S and vice-versa for the features $\nabla^2 H$ and A. Such assumption allows obtaining ROC curves whose area under the curve are greater than 0.5, that is the value associated to a completely random classifier.

It is necessary to underline that the objective function adopted in GM2 is the same of GM1. The main difference between the two methodologies is the fact that GM1 optimizes two parameters (n and τ), while GM2 works only on the relative value of the threshold trying to identify the best performing geomorphological feature.

The Figure 7.A and B describe the ROC curves associated with the linear binary classifiers obtained by separately thresholding each feature, defined in terms of false positive and true positive rates for both the Tiber River and the Chiascio sub-catchments. The graph provides a general description of the ability of each classifier in detecting flood prone areas.

For a quantitative evaluation of the results, we collected the values of the optimal normalized threshold, and the corresponding false positive rate r_{fp}, the true positive rate r_{tp}, the sum $r_{fp}+(1-r_{tp})$

obtained for each features, and the area under the ROC curve in Table 1 (for the Tiber River) and in Table 2 (for the Chiascio River) in order to objectively analyse the performance of the selected parameters that are *H*, *S* and *D*, respectively.

Along with the single feature classifier, linear binary classifiers as a function of two features were also tested. In this case 10 couples of normalized features (see Table 3 and 4) are considered using an index obtained by a linear combination of the two. Therefore, assigned the two normalized features x_1 and x_2, the algorithm adopts the following function for the classification:

$$S(\alpha_1 x_1 + \alpha_2 x_2 - \alpha_3) \qquad [4]$$

where: $S(\cdot)$ in the Heaviside step function, x_1 and x_2 are the considered normalized features, α_1 and α_2 the associated coefficients in the linear combination, and α_3 the threshold.

In order to simplify the search for the optimal parameters, the parameter space is reduced to two dimension assuming: $\alpha_1 = \cos(\theta)$, $\alpha_2 = \sin(\theta)$, $\alpha_3 = \mathrm{t}(\cos(\theta) + \sin(\theta))$, where $\theta \in [0, 2\pi)$ and $t \in [-1,1]$. Also in this case, the normalized threshold is obtained by minimizing the sum of the false positive rate and the false negative rate r_{fp} + (1 - r_{tp}).

The procedure is repeated for each of the 10 possible pairs of normalized features and the results for the optimal two-features binary classifiers, searched by discretizing θ and *t*, are summarized in Tables 3 and 4.

Once the optimal two-feature classifier has been identified, this classifier associates the pattern (x_1, x_2) to the class 0 if $\alpha_1^* x_1 + \alpha_2^* x_2 \leq \alpha_3$ to the class 1 otherwise. The corresponding ROC curve can be drawn varying the threshold α_3, while $\alpha_1 = \alpha_1^*$ and $\alpha_2 = \alpha_2^*$ are fixed.

The Figure 8.A and B compares the ROC curves associated with the best two-features classifiers and the best single-features classifiers previously obtained. Such comparison was used in order to understand if the linear combination of two features might produce some advantages with respect to the single feature classifier. Results shows that the best performing couple of parameters is represented by D and S in the Tiber River and H and D in the Chiascio River.

The two-feature classifier obviously provides a lower relative error measured by r_{fp} + (1 - r_{tp}). It identifies properly the 93% (and 85% for the Chiascio River) of flood-prone areas, with a reduction of the overestimation errors (r_{fn}) respect to the best single-feature. Nevertheless, the performances obtained with the single feature classifier based on relative elevation H alone are close to those obtained with the two-features in both river basins. Moreover, the H feature provides a slightly increase of r_{tp}, which means that identifies 93% (and 90% for the Chiascio River) of the areas exposed to flood inundation. Considering these aspects and the fact that the single feature classifier has the advantage to be simpler and requires less computational time, we adopted in the following the classifier based on the single feature H for comparison.

These results are consistent with those obtained in previous studies (Degiorgis et al., 2012) and confirm that increasing relative elevation from the risk source corresponds to lower hazard level. Another relevant advantage that one should underline in the use of the morphological feature H is the fact that the dimensionless threshold seems to be stable among the two selected study cases. This may be extremely useful when the flood map has to be extended in other sub-catchments of the same area.

4.3 The hydro-geomorphic delineation method

The third method is more complex, with respect to the first two, since it is based on advanced terrain analysis together with low frequency (return time higher than 200-500 years) flood flow heights and discharges, which are generally not available. The method is calibrated using the peak discharge at the basin outlet to estimate the hydraulic geometry parameters. As already explained in the previous paragraphs, this algorithm requires the value of peak discharge at the basin outlet; in the present case, this was set with reference to a return period of 200 years and extracted from the TRBA standard flood mapping plan and studies. In the present case, the values adopted for the peak discharge are 2700m^3/s and 1300 m^3/s for the Tiber River and the Chiascio at the outlet.

Figure 9 provides an example of the calibration of the method applied over the study area. In particular, the boundary of the hydro-geomorphic flooded area is compared with the standard TRBA flood map. There is a good agreement in general on the main river network with minor discrepancies that are clearly visible on the tributaries that are due to a misleading simulated stream network or due to the present of significantly urbanized areas. Such discrepancies in general are the result of the resolution of the DEM that is not able to accurately capture the morphology of the riverbanks, roads or other infrastructures. The overall performance of GM3 is presented in Figure 10.

4.4 Results comparison

To provide a visual comparison of the results of the three selected methods, maps of the areas exposed to flood inundations are visually compared with those predicted by the TRBA (Figure 11). In addition, Figure 12 provides a sequence of subsets of the global map in order to magnify the details of the results obtained by each procedure for two sample areas within the study domain. From the visual comparison, it is noted that the flood map obtained using GM1 is characterized by a larger flooded extent as compared to the other two methods, while GM3 seems to be less conservative.

Notwithstanding the limitation of the flood map adopted for comparison that may be affected by modelling errors and inaccuracies, it is necessary to state that such maps are probably the most accurate available over the area and it is very hard to obtain or find similar flood maps of real event at this scale. Therefore, this information was the only available over the Tiber River and according to our analysis the three methods provide a reasonable interpretation of areas subject to floods, highlighting the potential and performances of such geomorphic procedures, which can be easily applied and generalized over the entire river basin or large regions. Given the different level of complexity of the procedures adopted model intercomparison should take into account the number of parameters used for their calibration as well as the significantly different structure (see GM1 and GM2 versus GM3). This makes difficult the evaluation of the performances that have been measured by the same simple metrics introduced in the section 3.2. In particular, the values of r_{tp}, r_{fn}, r_{tn} and r_{fp} computed with the three different approaches are reported in Tables 5 and 6 for the two considered basins in order to provide a comprehensive and objective comparative analysis of the results.

These rates provides a measure of the ability of a model to correctly identify the flood areas (r_{tp}), to discriminate the portion an area that is free of flooding (r_{tn}), and the incorrect identification of flooded (r_{fp}) and non-flooded areas (r_{fn}). Results highlight the following aspects:

i) The sum of r_{fn} and r_{fp} provides a measure of the total error that allow a preliminary evaluation of the performances among methods. According this, the best performing method is the GM3 on the Upper Tiber River, while GM2 provides better results on the Chiascio river. This is a first preliminary indication on the scale effect on the different procedure adopted and it may be influenced by the resolution of the DEM adopted, which is probably too coarse for the smaller basin. Nevertheless, this limitation does not affect the performances of GM2 that improve significantly especially in terms of false positive rate.

ii) The GM1 shows the highest r_{tp} with a high r_{fp} false positive rate, while the GM2 shows a slightly lower r_{tp} and also a lower r_{fp} (especially for the Chiascio river). Both methods provide a small underestimation of the flooded areas that is certainly an important prerogative of a method for the delineation of flood prone areas.

iii) the GM3 shows a lower r_{tp} in both case studies, and the best performances in terms of r_{tn} and r_{fp} in both studied cases. This result may be partially related to the fact that the method was calibrated manually, but it is also due to the assumption of the model itself.

It is necessary to underline that GM2 somehow represents a generalization of GM1. In fact, it searches among a large number of morphological features in order to identify the best performing one. According to this, it seems that among all morphological features analysed in the present paper including the modified topographic index, the feature H seems to be the most significant for the identification of flood prone areas. This feature alone, after a binary classification, was able to beat the more complex GM3 on the Chiascio river.

This open a perspective for the use of such procedures that may be used to fill a gap in the flood mapping over the small scale basins. Such finding should be reinforced by additional studies that are currently undergoing, but it represents a great potential for the flood mapping over large scale that is currently limited to medium-large size basins.

After all, it is clear that each model has its own potential that can be optimized, using the information obtained from the present study, trying to understand how to improve these tools.

5 Conclusions

This study provides an investigation on the potential of three parsimonious geomorphic procedures emphasizing the role played by some morphologic features on flood exposure (e.g., elevation to the nearest channel, local slope, topographic convergence). The methodologies are tested on two sub-catchments of the Tiber River: one basin corresponds to the main river valley and one is an important tributary. Standard flood maps gathered from the TRBA are used for comparison purposes.

In the present application, the GM1 correctly identifies most of the flood prone areas, but it tends to overestimate their areal extension. The GM2 provides a lower r_{tp} value, but with a relevant reduction of r_{fp}. The GM3 seems not able to reach the same rate of true positive rate shown by the other two simpler methods, but it is more reliable in the identification of non-flooded area. In fact, it produces the highest r_{tn} value and the lower false positive rate, r_{fp}. GM3 is more impacted by the low resolution of the DEM, that seems inadequate to represent the flooded area morphology especially on upper tributaries and where urban features are significant.

Results of this comparative study show the main characteristics of the three selected methodologies emphasizing limitation and potential of each approach. In particular, it seems that methods based on morphological indices (GM1 as well as GM2) provides a better description of the valley bottom where flooded areas occur, but their performances are poorer in the identification of non-flooded areas where significant overestimation is noted. In this regard GM3 may play the important role of complementing the non-flooded characterization, since the hydro-geomorphic tool provides a very small overestimation error (both in terms of false negative rate and true negative rate) in defining the later extent of fluvial corridors. This result is mainly due to the fact that morphological indices are not able to detect the positive effect of riverbanks and other artefact. To be noted that GM3 seems to be sensitive to the DEM resolution and its performances shall surely benefit of the increasing availability of more accurate and detailed DEM that new technologies will make available in the near future.

As a result, the coupling of next generation digital topographic data with a new integrated terrain analysis tool integrating an optimal combination of the three selected procedures may pave the efficient use of DEM-based morphological approaches for a more reliable classification of flood risk over large areas. Furthermore, it would be extremely interesting to try identifying a possible relationship between the threshold values of the GM1 or GM2 procedures as a function of the different return period of the flood inundations.

References

1. Arnaud-Fassetta, G., Astrade, L., Bardou, E., Corbonnois, J., Delahaye, D., Fort, M., Gautier, E., Jacob, N., Peiry, J.L., Piégay, H., Penven, M.J., 2009. Fluvial geomorphology and flood-risk management, *Geomorphologie*, 2, 109-128.
2. Beven, K.J., Kirkby, M.J., Schoffield, N., & Tagg, A., 1984. Testing a physically-based flood forecasting model (TOPMODEL) for three UK catchments, *J. Hydrol.*, 69, 119-143.
3. Burt, T.P., & Butcher, D.P., 1986. Development of topographic indices for use in semidistributed hillslope runoff models, in Geomorphology and Land Management, edited by D. Baltenau and O. Slaymaker, Z., Geomorphol. Suppl. Band, 58, 1-19.
4. Calenda, G., C.P. Mancini, E. Volpi, 2005. Distribution of the extreme peak floods of the Tiber River from the XV century, *Advances in Water Resources*, 28(6), 615-625.
5. Cobby, D.M., Mason, D.C., Horritt, M.S., Bates, P.D., 2003. Two-dimensional hydraulic flood modelling using a finite-element mesh decomposed according to vegetation and topographic features derived from airborne scanning laser altimetry, *Hydrol. Process.*, 17(10).
6. Degiorgis, M., Gnecco, G., Gorni, S., Roth, G., Sanguineti, M., Taramasso, A.C. 2012. Classifiers for the detection of flood-prone areas using remote sensed elevation data, *J. Hydrol.*, 470-471, 302–315.
7. Degiorgis, M., Gnecco, G., Gorni, S., Roth, G., Sanguineti, M., Taramasso A.C., 2013. Flood hazard assessment via threshold binary classifiers: The case study of the Tanaro River Basin, *Irrig. Drain.*, 62(2): 1-10, doi:10.1002/ird.1806.
8. Di Baldassarre, G., Schumann, G.J.-P., Bates, P.D. 2009. Near real time satellite imagery to support and verify timely food modelling. *Hydrol. Process.*, 23, 799-803.
9. Di Baldassarre, G., Kooy, M., Kemerink, J. S., and Brandimarte, L., 2013a. Towards understanding the dynamic behaviour of floodplains as human-water systems, *Hydrol. Earth Syst. Sci.*, 17, 3235-3244, doi:10.5194/hess-17-3235-2013.
10. Di Baldassarre, G., Viglione, A., Carr, G., Kuil, L., Salinas, J. L., and Blöschl, G., 2013b. Socio-hydrology: conceptualising human-flood interactions, *Hydrol. Earth Syst. Sci.*, 17, 3295-3303, doi:10.5194/hess-17-3295-2013.

11. Di Leo, M., Manfreda, S., Fiorentino, M. 2011. An automated procedure for the detection of flood prone areas: r.hazard.flood, Geomatics Workbooks n. 10 - "FOSS4G-it: Trento 2011", 83-89.
12. Dilley, M., R.S. Chen, U. Deichmann, A.L. Lerner-Lam, M. Arnold, J. Agwe, P. Buys, O. Kjekstad, B. Lyon, and G. Yetman. 2005. Natural Disaster Hotspots: A Global Risk Analysis. Disaster Risk Management Series No. 5. Washington, D.C.: The World Bank.
13. Dodov, B.A., and Foufoula-Georgiou, E., 2006. Floodplain Morphometry Extraction From a High-Resolution Digital Elevation Model: A Simple Algorithm for Regional Analysis Studies, *IEEE Geosci. Remote S*, 3(3).
14. Fawcelt, T. 2006. "An Introduction to ROC Analysis". Pattern Recognition Letters 27 (8): 861–874. doi:10.1016/j.patrec.2005.10.010.
15. Gallant, J. C., and Dowling, T. I. 2003. A multiresolution index of valley bottom flatness for mapping depositional areas, *Water Resour. Res*., 39(12), 1347, doi:10.1029/2002WR001426.
16. Giannoni, F., Roth, G., Rudari, R., 2005. A procedure for drainage network identification from geomorphology and its application to the prediction of the hydrologic response. *Adv. Water Resour.*, 28, 567–581.
17. Grimaldi S, Petroselli, A., Arcangeletti, E., Nardi, F., 2013. Flood mapping in ungauged basins using fully continuous hydrologic-hydraulic modelling. *J. Hydrol*., vol. 487 , p. 39-47.
18. Jalayer, F., Derisi, R., Depaola, F., Giugni, M., Manfredi, G., Gasparini, P., Topa, M. E., Yonas, N., Yeshitela, K., Nebebe, A., Cavan, G., Lindley, S., Printz, A. & Renner, F. Probabilistic GIS-based method for delineation of flood-prone areas and identification of urban hotspots, Published in Online First in Natural Hazards. 10.1007/s11069-014-1119-2
19. Horritt, M.S., Bates P.D., 2002. Evaluation of 1D and 2D numerical models for predicting river flood inundation, *J. Hydrol.*, 268 (1–4), Pages 87-99.
20. Jenson, S.K., & Domingue J.O., 1988. Extracting Topographic Structure from Digital Elevation Data for Geographic Information System Analysis. *Photogramm Eng Rem S*, 54 (11): 1593-1600.
21. Kirkby, M.J., 1975. Hydrograph modelling strategies. *Progress Phys. Hum. Geogr*, 69–90,.

22. Kim, J., Ivanov, V. Y. Warnock, A., and Katopodes, N., 2011. Coupled modeling of hydrologic and hydrodynamic processes including overland and channel flow, *Adv. Water Resour.*, doi:10.1016/j.advwatres.2011.11.009.

23. Lamb, R., M. Crossley, S. Waller, A fast two-dimensional floodplain inundation model, Proceedings of the ICE - Water Management, 162(6), 363 –370, 2009

24. Manfreda, S., Di Leo, M., Sole, A., 2011. Detection of Flood Prone Areas using Digital Elevation Models, *J. Hydrol. Eng.*, 16(10), 781-790.

25. McGlynn, B. L., & Seibert, J. 2003. Distributed assessment of contributing area and riparian buffering along stream networks, *Water Resour. Res.*, 39(4), 1082, doi: 10.1029/2002WR001521.

26. Montgomery, D. R., and W. E. Dietrich, 1988. Where do channels begin?, *Nature*, 336, 232-234.

27. Moore, I.D., Grayson, R.B., & Ladson, A.R., 1991. Digital terrain modelling: A review of hydrological, geomorphological, and biological applications, *Hydrol. Process.*, 5: 3–30.

28. Nardi, F., Vivoni, E.R., Grimaldi, S., 2006. Investigating a floodplain scaling relation using a hydrogeomorphic delineation method, *Water Resour. Res.*, 42, W09409.

29. Nardi, F., Grimaldi, S., Petroselli, A., Santini, M., Ubertini, L., 2008. Hydrogeomorphic properties of simulated drainage patterns using DEMs: the flat area issue, *Hydrolog. Sci. J.*, 53(6) doi: 10.1623/hysj.53.6.1176

30. Nardi, F., Biscarini, C., Di Francesco, S., Manciola, P., Ubertini, L., 2013. Comparing a large-scale DEM-based floodplain delineation algorithm with standard flood maps: the Tiber river basin case study, Irrigation and Drainage, VL - 62, IS - S2, DO - 10.1002/ird.1818.Pappenberger, F., Dutra, E., Wetterhall, F., and Cloke, H. L.: Deriving global flood hazard maps of fluvial floods through a physical model cascade, *Hydrol. Earth Syst. Sci.*, 16, 4143-4156, doi:10.5194/hess-16-4143-2012, 2012.

31. Sivapalan, M., Savenije, H. H. G. and Blöschl, G., 2012. Socio-hydrology: A new science of people and water. *Hydrol. Process.*, 26: 1270–1276. doi: 10.1002/hyp.8426

32. Tucker, G.E., Lancaster, S.T., Gasparini, N.M., and Bras, R.L., 2001. *The Channel-Hillslope Integrated Landscape Development (CHILD) Model*, in Landscape Erosion and Evolution Modeling, edited by R.S. Harmon and W.W. Doe III, Kluwer Academic/Plenum Publishers, pp. 349-388.

33. Tucker, G.E., and Whipple, K.X., 2002. Topographic outcomes predicted by stream erosion models: Sensitivity analysis and intermodel comparison, *J. Geophys. Res.*, 107(B9), 2179, 10.1029/2001JB000162.

34. Werner, M., Blazkova, S., Petr, J., 2005. Spatially distributed observations in constraining inundation modelling uncertainties. *Hydrol. Process.*, 19, 3081-3096.

35. Williams, W.A., Jensen, M.E., Winne, J.C., & Redmond, R.L., 2000. An automated technique for delineating and characterizing valley-bottom settings, *Environ. Monit. Assess.*, 64, 105-114.Winsemius, H. C., Van Beek, L. P. H., Jongman, B., Ward, P. J., and Bouwman, A.: A framework for global river flood risk assessments, *Hydrol. Earth Syst. Sci.*, 17, 1871-1892, doi:10.5194/hess-17-1871-2013, 2013.

TABLES

Features	τ	r_{fp}	r_{tp}	r_{fp}+(1-r_{tp})	AUC
As	-0.999	0.013	0.108	0.905	0.548
D	-0.982	0.298	0.759	0.539	0.799
∇^2H	0.018	0.731	0.930	0.802	0.543
H	**-0.952**	**0.336**	**0.934**	**0.402**	**0.867**
S	-0.943	0.412	0.935	0.476	0.800

Table 1. Upper Tiber River basin. The threshold, τ, the false positive rate, r_{fp}, the true positive rate, r_{tp}, the sum $r_{fp} + (1 - r_{tp})$, and the area under the curve (AUC) for the five selected features. The best performing feature is highlighted using bold characters.

Features	τ	r_{fp}	r_{tp}	r_{fp}+(1-r_{tp})	AUC
As	-0.999	0.058	0.276	0.783	0.614
D	-0.960	0.150	0.835	0.315	0.906
∇^2H	-0.017	0.744	0.932	0.813	0.579
H	**-0.956**	**0.188**	**0.901**	**0.286**	**0.935**
S	-0.929	0.442	0.877	0.565	0.746

Table 2. Chiascio River basin. The threshold, τ, the false positive rate, $\mathbf{r_{fp}}$, the true positive rate, $\boldsymbol{r_{tp}}$, the sum $\boldsymbol{r_{fp} + (1 - r_{tp})}$, and the area under the curve (AUC) for the five selected features. The best performing feature is highlighted using bold characters.

Pairs of features	**θ***	**t***	**r_{fp}**	**r_{tp}**	**r_{fp}+(1-r_{tp})**
As, D	310	-0.900	0.263	0.724	0.539
As, ∇^2H	90	0.020	0.731	0.930	0.802
As, S	310	-0.640	0.412	0.938	0.474
As, H	310	-0.700	0.337	0.934	0.402
∇^2H, S	230	-0.500	0.356	0.901	0.456
∇^2H,H	260	-0.800	0.359	0.950	0.409
D, ∇^2H	180	-0.980	0.331	0.791	0.541
D, S	**210**	**-0.960**	**0.287**	**0.930**	**0.356**
D, H	240	-0.960	0.301	0.928	0.374
H, S	210	-0.960	0.262	0.889	0.373

Table 3. Upper Tiber River. The θ* and t* parameters, the false positive rate $\boldsymbol{r_{fp}}$, the true positive rate $\boldsymbol{r_{tp}}$, the sum $\boldsymbol{r_{fp} + (1 - r_{tp})}$ and the area under the curve AUC for the approximately optimal two features linear binary classifiers. The best performing parameters is highlighted using bold characters.

Pairs of features	$\boldsymbol{\theta}$*	t*	r_{fp}	r_{tp}	r_{fp}+(1-r_{tp})
As, D	270	-0.960	0.150	0.835	0.315
As, ∇^2H	40	-0.540	0.520	0.726	0.794
As, S	290	-0.880	0.442	0.881	0.561
As, H	300	-0.900	0.161	0.877	0.284
∇^2H, S	250	-0.680	0.405	0.850	0.555
∇^2H,H	270	-0.960	0.139	0.842	0.297
D, ∇^2H	180	-0.960	0.149	0.834	0.315
D, S	190	-0.940	0.173	0.884	0.289
D, H	**230**	**-0.960**	**0.098**	**0.850**	**0.248**
H, S	180	-0.960	0.139	0.843	0.296

Table 4. Chiascio River basin. The θ* and t* parameters, the false positive rate $\boldsymbol{r_{fp}}$, the true positive rate $\boldsymbol{r_{tp}}$, the sum $\boldsymbol{r_{fp} + (1 - r_{tp})}$ and the area under the curve AUC for the approximately optimal two features linear binary classifiers. The best performing parameters is highlighted using bold characters.

670

	Mod. Topographic	Single-feature	Hydrogeomorphic	Ideal value
True positive rate, r_{tp}	93.8%	93.4%	75.8%	100%
False negative rate, r_{fn}	6.2%	6.6%	24.2%	0%
True negative rate, r_{tn}	61.3%	66.4%	94.3%	100%
False positive rate, r_{fp}	38.7%	33.6%	5.7%	0%
$r_{fn} + r_{fp}$	44.9%	40.2%	29.9%	0%

671 **Table 5.** Comparison among the three investigated methods in terms of statistical measures of the

672 performances for the Upper Tiber Basin.

	Mod. Topographic	Single-feature	Hydrogeomorphic	Ideal value
True positive rate, r_{tp}	90.2%	90.1%	60.1%	100%
False negative rate, r_{fn}	9.8%	9.9%	39.9%	0%
True negative rate, r_{tn}	51.4%	81.2%	97.2%	100%
False positive rate, r_{fp}	48.6%	18.8%	2.8%	0%
$r_{fn} + r_{fp}$	58.4%	28.7%	42.7%	0%

Table 6. Comparison among the three investigated methods in terms of statistical measures of the performances for the Chiascio River basin.

FIGURES

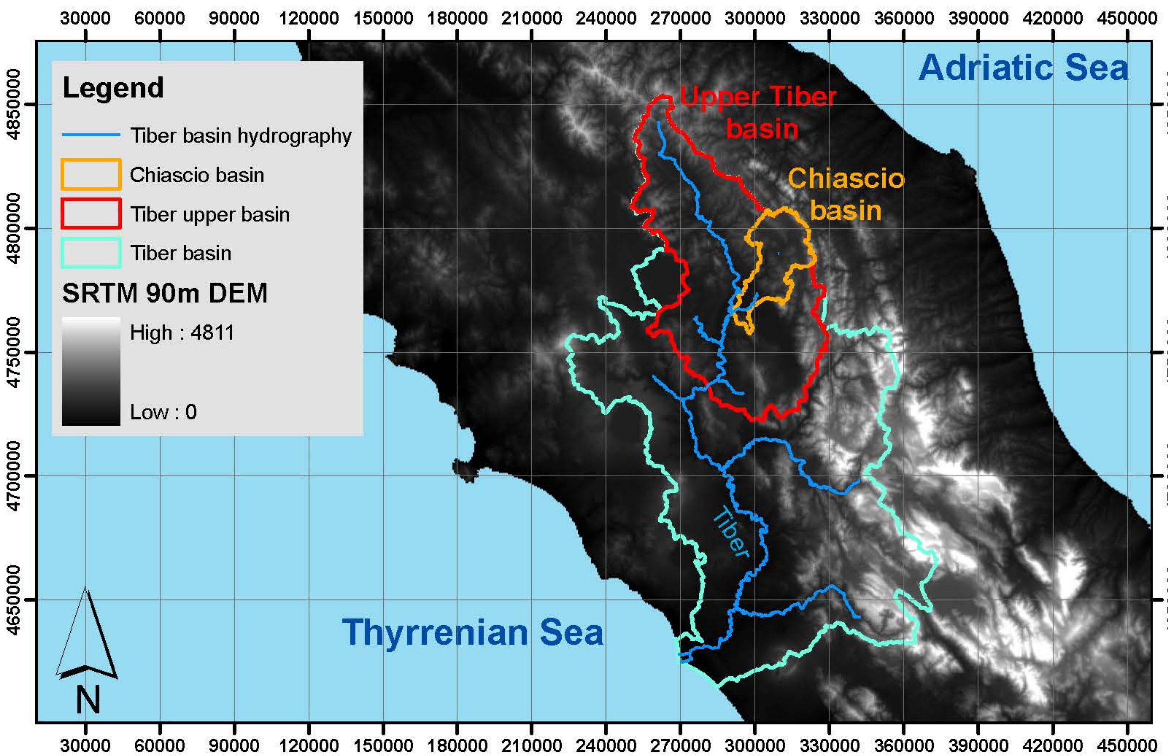

Figure 1. Tiber River geographic and topographic setting in Central Italy. The two selected study basins are located in the upper Tiber upstream of the Lazio-Umbria boundaries. The Chiascio river is a left tributary (in orange)..

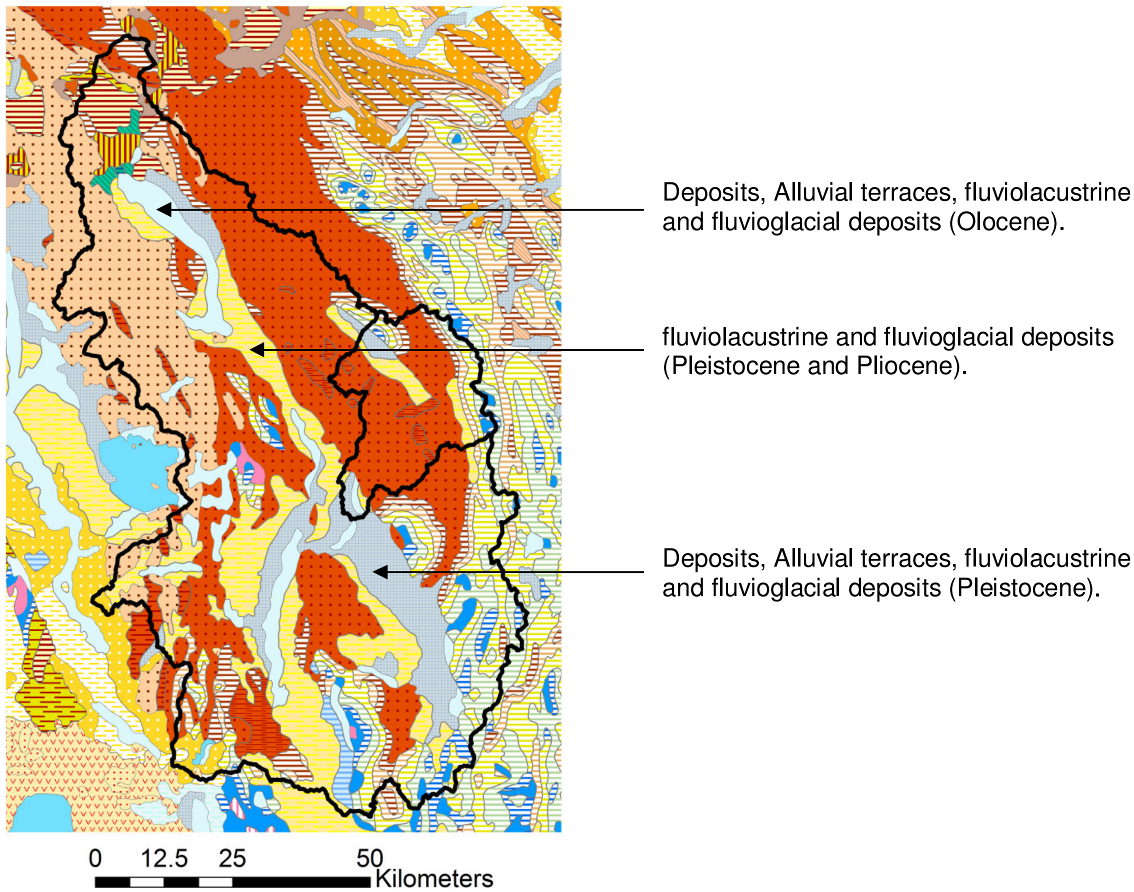

Figure 2. Identification of the alluvial plain based on the geological map of the Upper Tiber River.

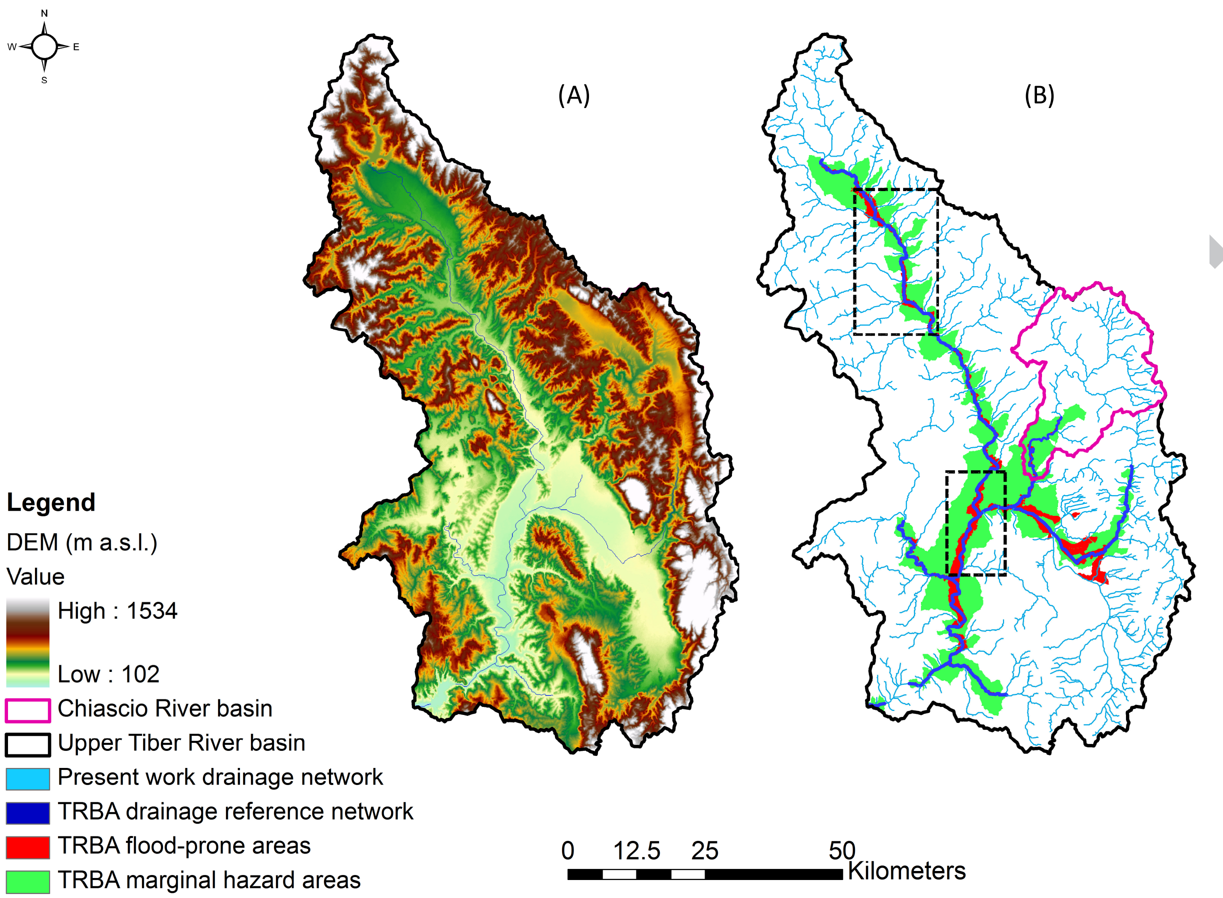

Figure 3. A) Filled Digital Elevation Model (m a.s.l) derived from SRTM data. B) Summary of the Tiber Basin Authority studies: reference drainage network (dark blue), flood-prone areas (red), and marginal hazard areas (green). The dashed boxes describe insets used for a local comparison of the proposed procedures.

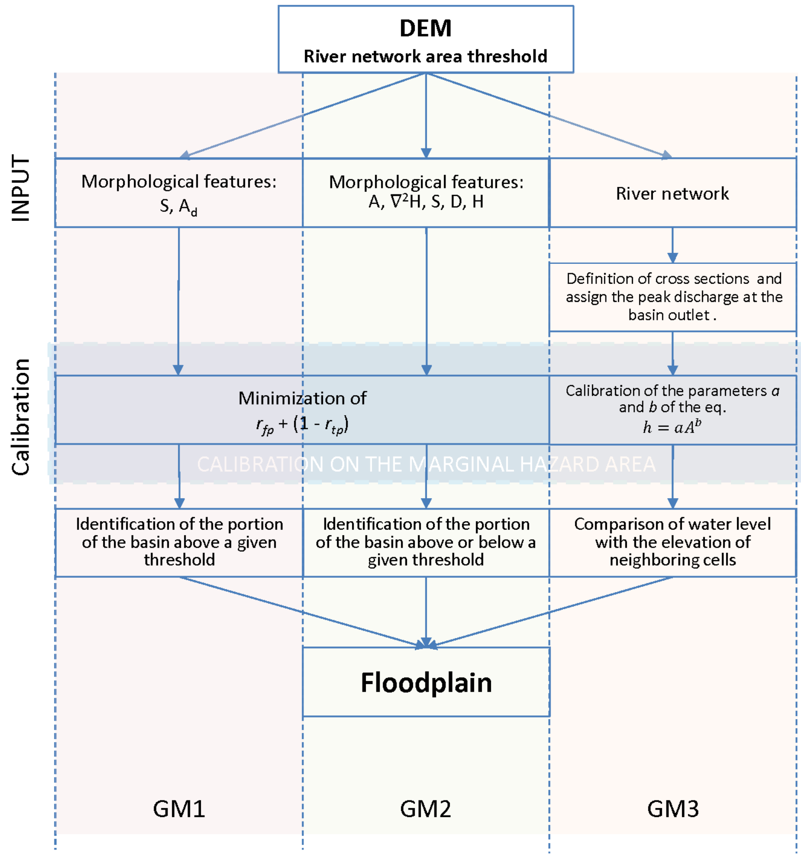

Figure 4. Schematic description of the three different algorithms analysed herein.

697

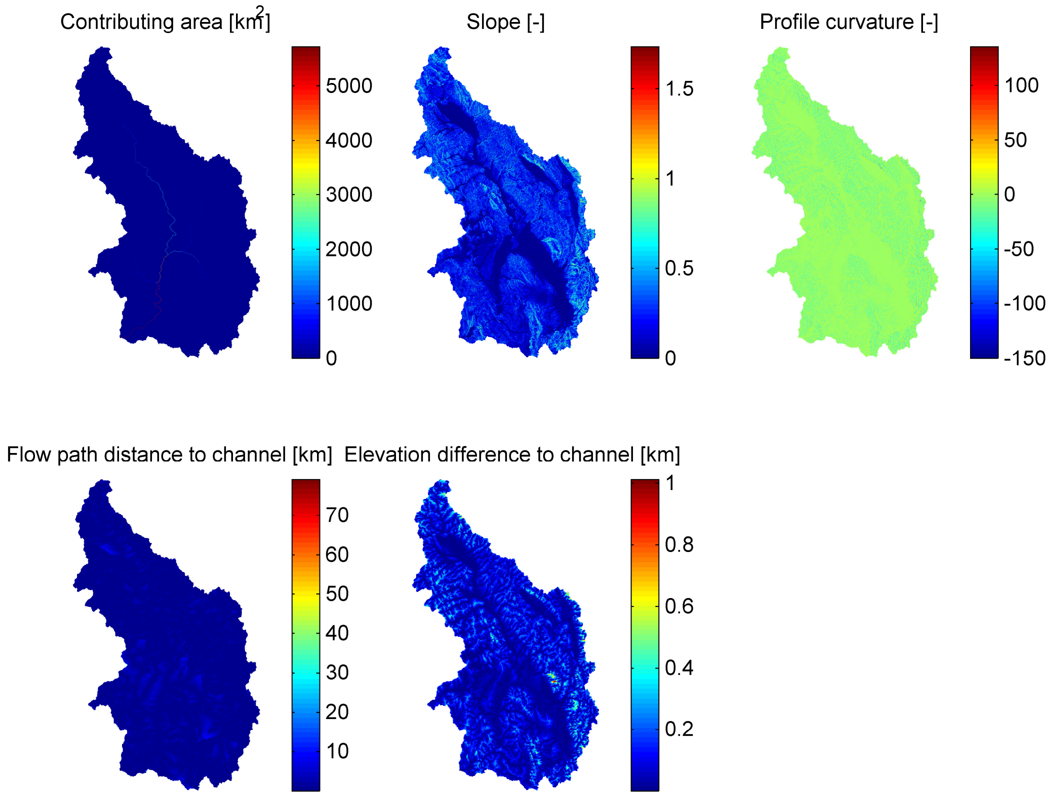

698

699 **Figure 5.** Representation of the basic morphologic features used to identify flood-prone areas of

700 the Upper Tiber River with the GM2 approach.

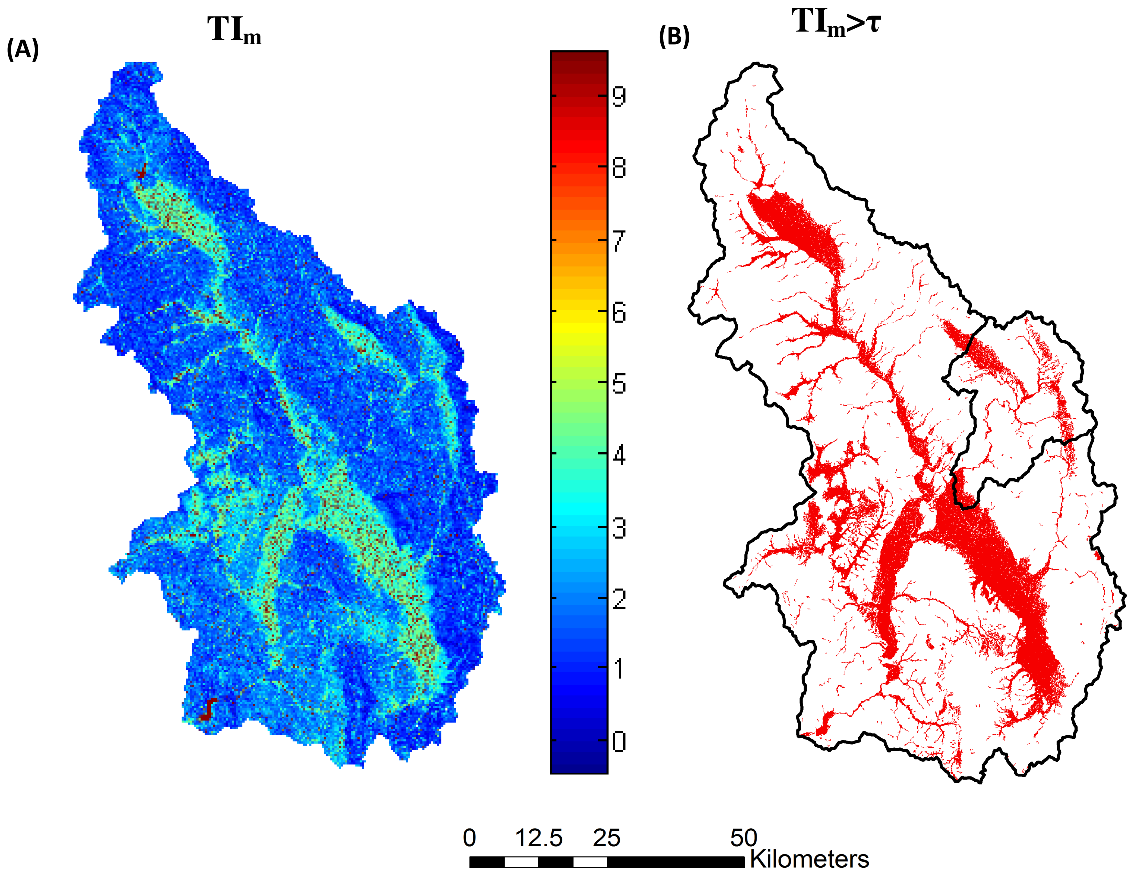

Figure 6. A) Maps of the Modified Topographic Index and B) maps of the sub-catchment areas exposed to flood inundations according to this method; for the Upper Tiber River τ=3.1, for the Chiascio River τ=2.6).

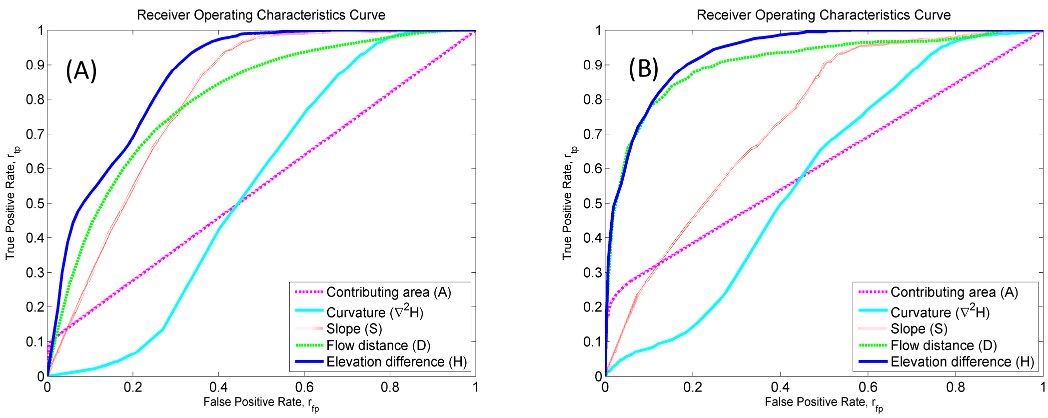

Figure 7. Receiver Operating Characteristics (ROC) curves for the five selected features for the Upper Tiber River basin (A) and the Chiascio River basin (B). ROC curves are obtained by applying a threshold to one of the five features in the dataset, and by varying the threshold.

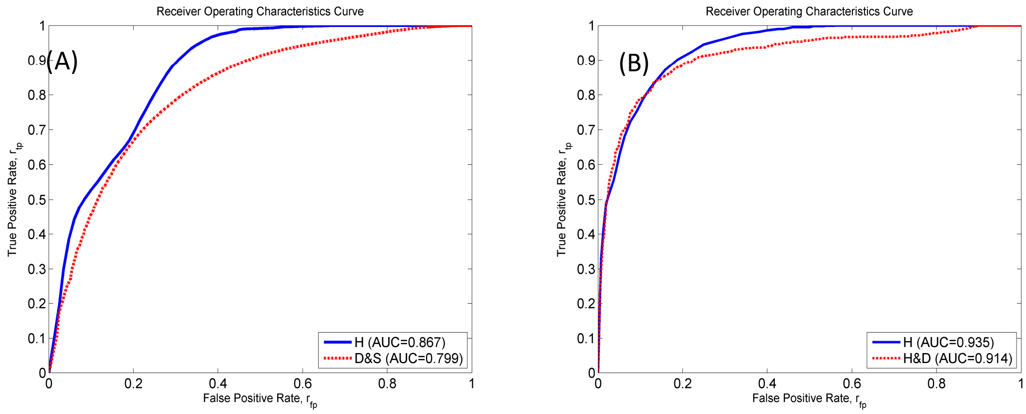

Figure 8. Receiver Operating Characteristics (ROC) curve and area under the curve (AUC) for the best two-features classifier, based on the flow path distance to the nearest stream and slope S for the Upper Tiber River basin (A) and the Chiascio River basin (B). ROC curves and AUCs for the best single-features classifiers based on H is also reported.

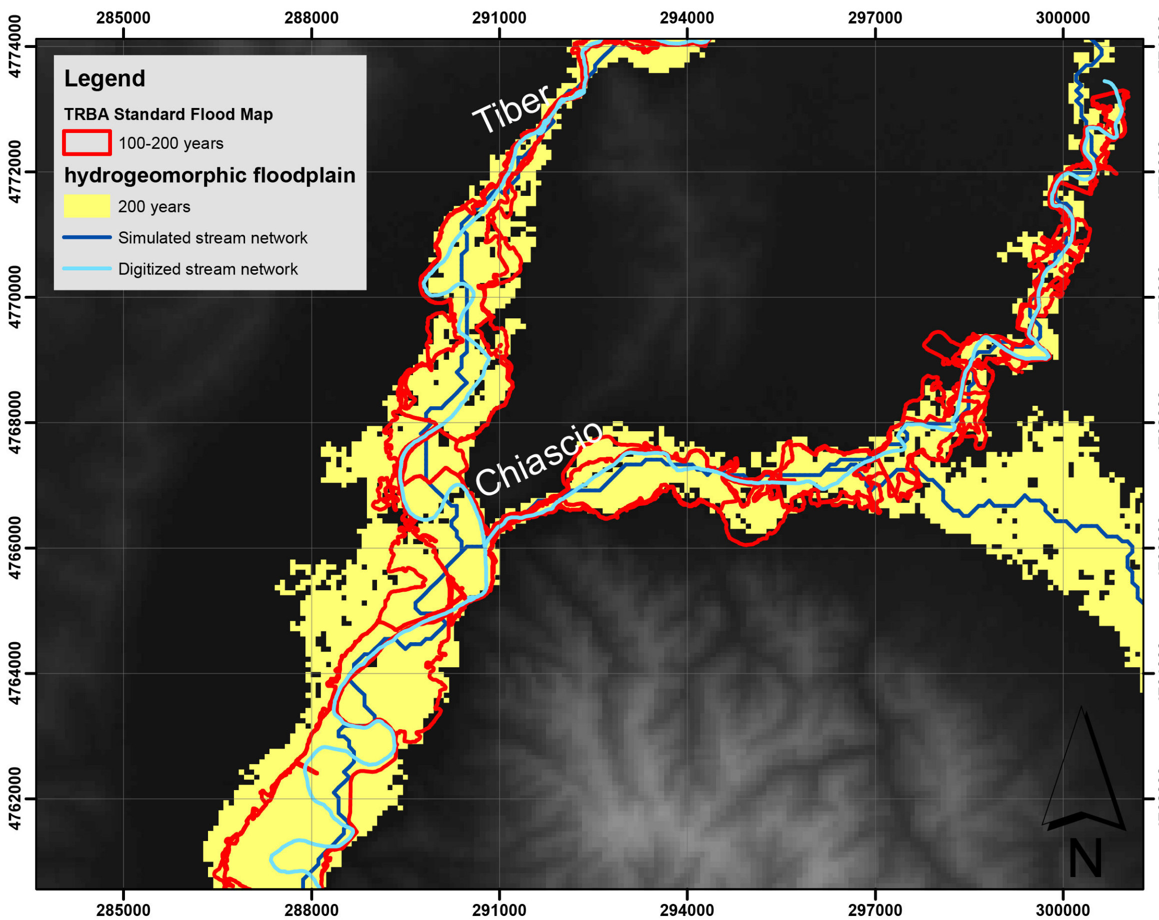

Figure 9. Identification of flood prone area using the GM3 model: calibration by qualitative comparison with the standard flood map on the Tiber-Chiascio confluence area.

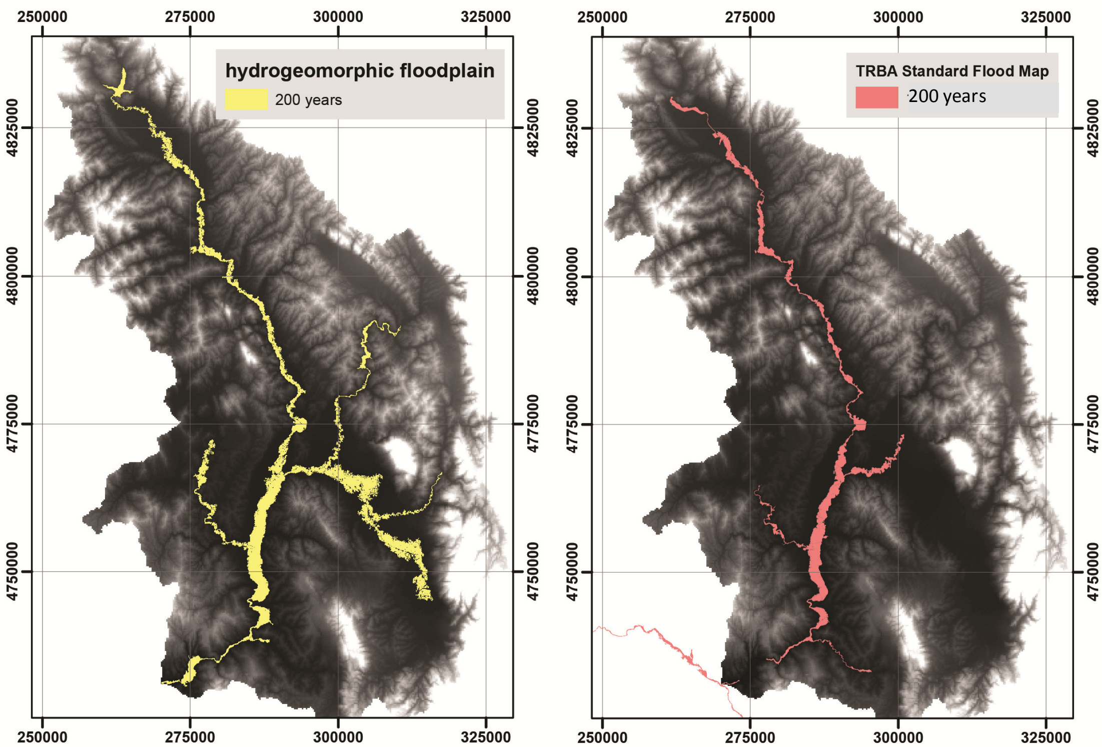

Figure 10. Hydro-geomorphic flooded area delineation results (GM3 model) on the study area as compared to standard TRBA flood map for 200 years return time

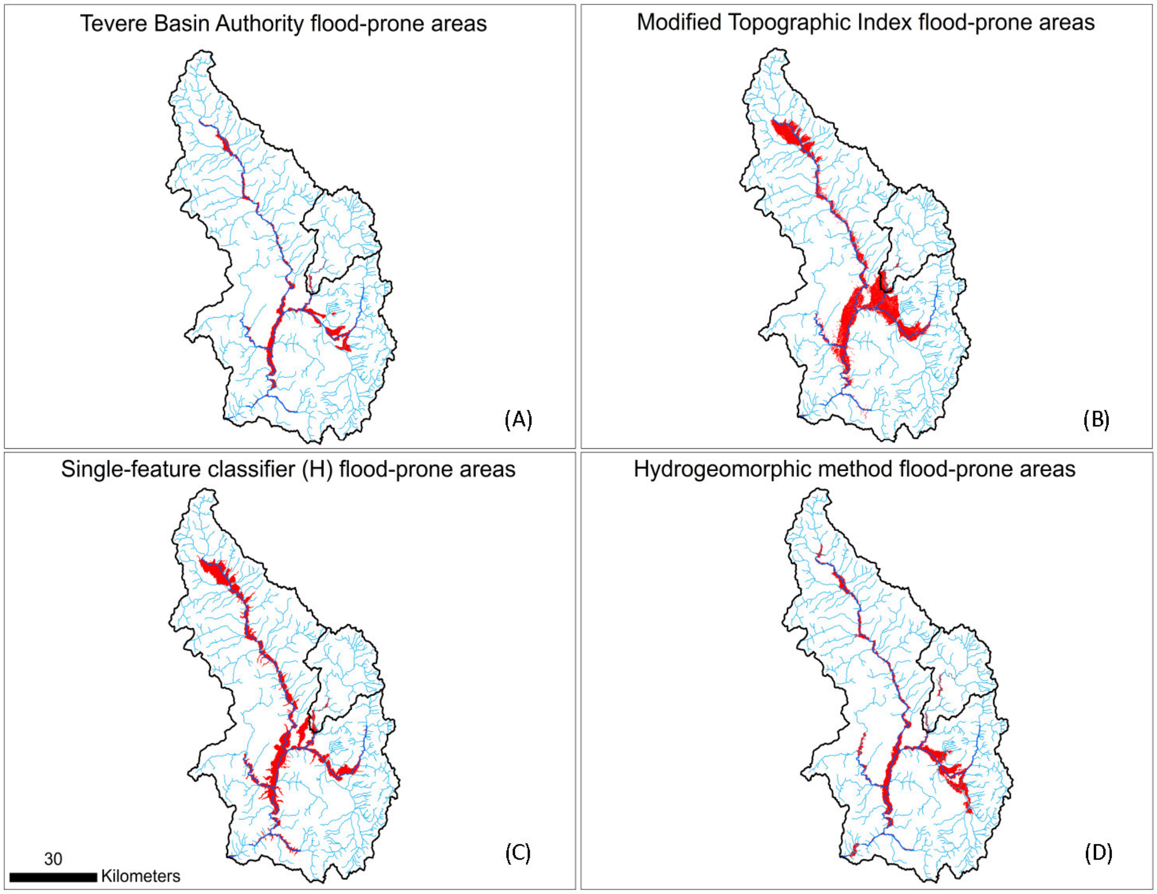

Figure 11. Maps of the areas exposed to flood inundations according to the three mentioned methodologies (B, C, and D), compared with those predicted by the Tiber River Basin Authority (A).

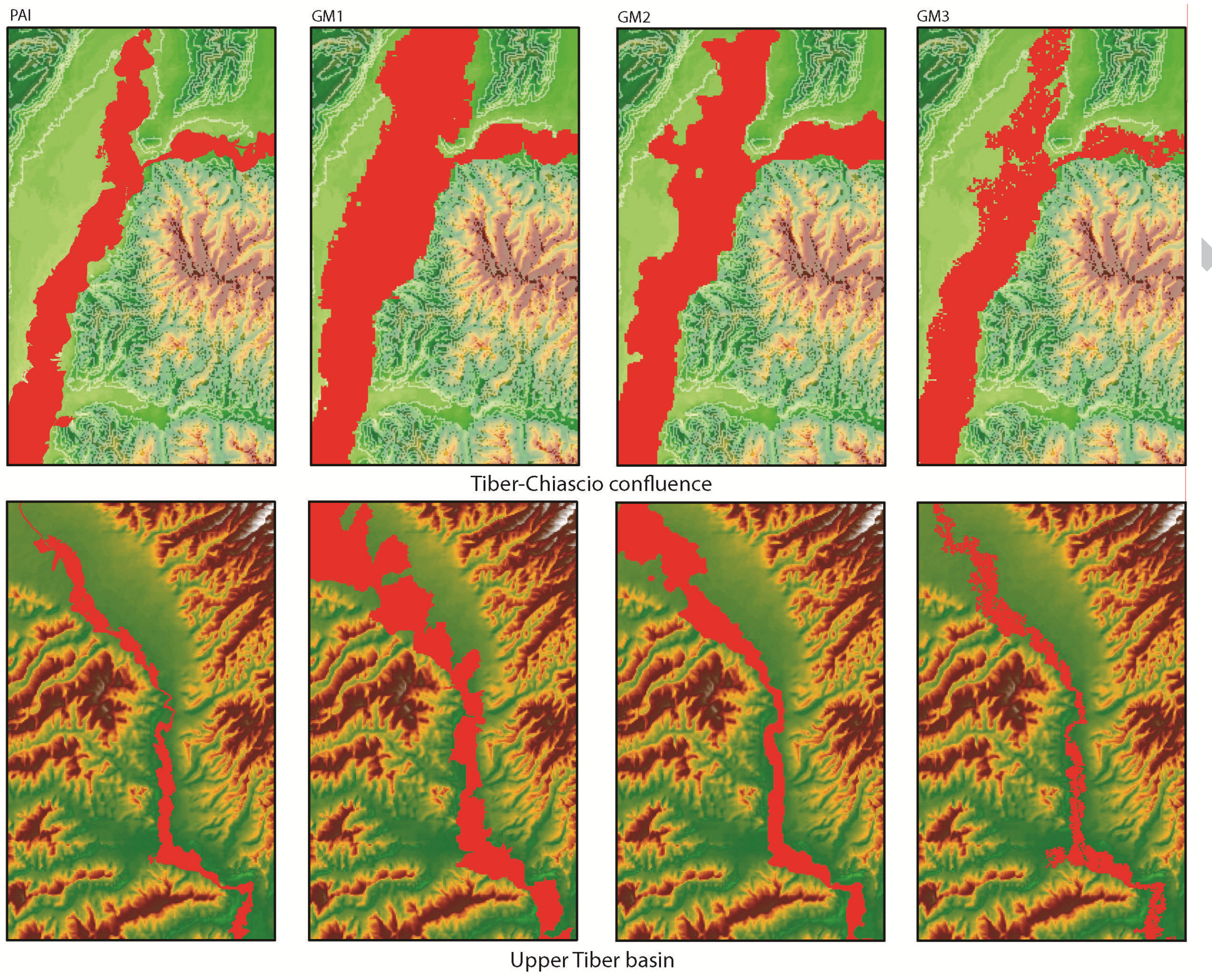

Figure 12. Visual comparison of the performances of the GM1, GM2 and GM3 methods as compared to standard TRBA PAI flood maps for two different areas: the upper basin (upper boxes) and the Tiber-Chiascio confluence zone (lower boxes).

Highlights

Mapping flood hazard on the Tiber River.

Comparative analysis of three different geomorphic approaches for the identification of flood prone areas.

New strategies for preliminary flood hazard mapping in ungauged basins.